The Death Receptor 3–TNF-like protein 1A pathway drives adverse bone pathology in inflammatory arthritis

Melanie Jane Bull,[1] Anwen Siân Williams,[2] Zarabeth Mecklenburgh,[1] Claudia Jane Calder,[1] Jason Peter Twohig,[1] Carole Elford,[3] Bronwen Alice James Evans,[3] Tania F. Rowley,[4] Tomasz J. Slebioda,[4] Vadim Y. Taraban,[4] Aymen Al-Shamkhani,[4] and Eddie Chung Yern Wang[1]

[1]Department of Medical Biochemistry and Immunology, [2]Department of Rheumatology, and [3]Department of Child Health, School of Medicine, Heath Park, Cardiff CF14 4XN, Wales, UK
[4]Cancer Sciences Division, University of Southampton School of Medicine, Southampton SO16 6YD, England, UK

Rheumatoid arthritis (RA) is a chronic inflammatory disease of synovial joints that is associated with cartilage and bone destruction. Death Receptor 3 (DR3), a tumor necrosis factor (TNF) receptor superfamily member, has recently been associated with the pathogenesis of RA. We demonstrate that absence of DR3 confers resistance to the development of adverse bone pathology in experimental antigen-induced arthritis (AIA). DR3^{ko} mice exhibited a reduction in all histopathological hallmarks of AIA but, in particular, failed to develop subchondral bone erosions and were completely protected from this characteristic of AIA. In contrast, TNF-like protein 1A (TL1A), the ligand for DR3, exacerbated disease in a dose- and DR3-dependent fashion. Analysis of osteoclast number within AIA joint revealed a reduction in areas susceptible to bone erosion in DR3^{ko} mice, whereas in vitro osteoclastogenesis assays showed that TL1A could directly promote osteoclastogenesis in mouse and man. Treatment with antagonistic anti-TL1A mAb protected animals in a systemic model of RA disease collagen-induced arthritis. We therefore conclude that the DR3–TL1A pathway regulates joint destruction in two murine models of arthritis and represents a potential novel target for therapeutic intervention in inflammatory joint disease.

CORRESPONDENCE
Eddie Chung Yern Wang:
WangEC@cf.ac.uk

Rheumatoid arthritis (RA) is a chronic inflammatory disease affecting ~1% of the global population (1). RA is characterized by infiltration of synovial joints by immune cells, principally macrophages, T cells, plasma cells, and hyperplasia of the synovial lining. This eventually results in the destructive phase of disease causing damage to cartilage and bone. It is widely accepted that cytokines and their receptors play a central role in the pathogenesis of RA, thus TNFα, IL-1, and IL-6 have been identified as key mediators of the disease (2–4). The role played by members of the TNF receptor superfamily (TNFRSF) in pathological bone resorption has also become widely accepted, with RANK and RANKL acting as crucial factors in differentiation of osteoclasts (5), the primary cell type involved in bone degradation.

DR3 (TRAMP, LARD, Apo3, Wsl1, and TNFRSF25) is a member of the TNFRSF and shows closest homology to TNFR1 (6). Like TNFR1, DR3 contains four extracellular cysteine-rich repeats and is capable of signaling both apoptosis via caspase 8 activation and cell survival via the activation of NFκB (7–9). The biological function of DR3 is an area of growing interest. In the immune system, DR3 has been shown to affect negative selection during thymocyte development (10) and can modulate T cell (11–13) and NKT cell function (14). It has also been associated with inflammatory diseases such as irritable bowel disease (15, 16) and atherosclerosis (17). Interestingly, DR3,

M.J. Bull and A.S. Williams contributed equally to this paper.

The Rockefeller University Press $30.00
J. Exp. Med. Vol. 205 No. 11 2457-2464
www.jem.org/cgi/doi/10.1084/jem.20072378

The Journal of Experimental Medicine

along with its only known ligand, TNF-like protein 1A (TL1A) (18), has been linked with RA. Duplication of the DR3 gene is more prevalent in RA patients compared with controls (19), whereas TL1A$^+$ mononuclear phagocytes have been identified in rheumatoid synovium and soluble TL1A has been detected in synovial fluid of patients (20). However, functional analysis of the in vivo role of the DR3–TL1A pathway in RA has not yet been reported.

To address this, we have generated mice lacking the DR3 gene (DR3^{ko}) on a C57BL/6 background (10) and used a salient model of experimental arthritis to elucidate functional aspects of DR3 activity. Antigen-induced arthritis (AIA) is a local model of disease which displays many pathological features of RA including cellular infiltration, synovial hyperplasia, pannus formation, cartilage depletion, and bone destruction (21). We show that DR3 is essential for the development of adverse joint pathology in AIA and that anti-TL1A treatment can protect from the systemic model of disease, collagen-induced arthritis (CIA). These results imply an important in vivo function for DR3 in the pathogenesis of inflammatory arthritis and provide proof of principle that countering this pathway may represent a novel therapy for RA.

RESULTS AND DISCUSSION

DR3^{ko} mice show reduced inflammatory response to AIA compared with DR3^{wt} controls

To investigate the in vivo role of DR3 in inflammatory arthritis, we induced AIA in DR3^{ko} mice and DR3^{wt} controls. All mice developed an inflammatory reaction in response to intraarticular injection of methylated BSA, with both DR3^{ko} and DR3^{wt} mice exhibiting a similar pattern of joint swelling over a 21-d time course. Comparable knee joint swelling measurements were noted in DR3^{ko} and DR3^{wt} mice at the peak of response, 1 d after mBSA injection. Thereafter, swelling resolved in both but faster in the absence of DR3 (Fig. 1 A).

We next assessed whether more rapid resolution of joint swelling was translated to improved pathological outcome in DR3^{ko} mice. Examination of histopathological severity was performed on joint sections taken during the acute inflammatory phase when TNFα, IL-1β, and IL-6 reach a peak and destructive pathology first becomes detectable (3 d after induction) and when there is maximal evidence of structural damage within the joint (21 d after induction) (21). The severity of arthritis (arthritis index [AI]) was quantified in hematoxylin and eosin (H&E)–stained sections by grading parameters as described in Materials and methods. On day 3 after arthritis induction, DR3^{wt} (Fig. 1 B) and DR3^{ko} mice (Fig. 1 C) did not differ histopathologically. By day 21, DR3^{wt} mice had developed arthritis characterized by extensive cellular infiltration, synovial hyperplasia, formation of a thick pannus, and bone erosions (Fig. 1 D). In contrast, DR3^{ko} mice displayed mild pathological features of arthritis, showing general absence of synovial hyperplasia, lack of pannus formation, and no evidence of bone erosion (Fig. 1 E). Indeed, all scoring parameters were either absent or significantly milder in DR3^{ko} compared with DR3^{wt} mice (Fig. 1 F). This translated into a significant reduction in the AI (Fig. 1 G).

As a second outcome measure of structural damage to the joint, we assessed proteoglycan depletion from articular cartilage on the femoral head using Safranin O/Fast Green staining 21 d after arthritis induction. In DR3^{wt} mice, cartilage was severely depleted, as illustrated by lack of red Safranin O staining resulting in an obvious tidemark (Fig. 1 H). DR3^{ko} mice did not display much cartilage depletion (Fig.1 I), retaining similar levels of Safranin O staining as nonarthritic control left knees (not depicted). Collectively, this data indicate that there is considerable protection against degenerative AIA disease pathology in DR3^{ko} mice.

TL1A exacerbates disease in a DR3-dependent fashion

To confirm that resistance to AIA was DR3 specific, TL1A was injected with mBSA on day 0 of the AIA model at escalating

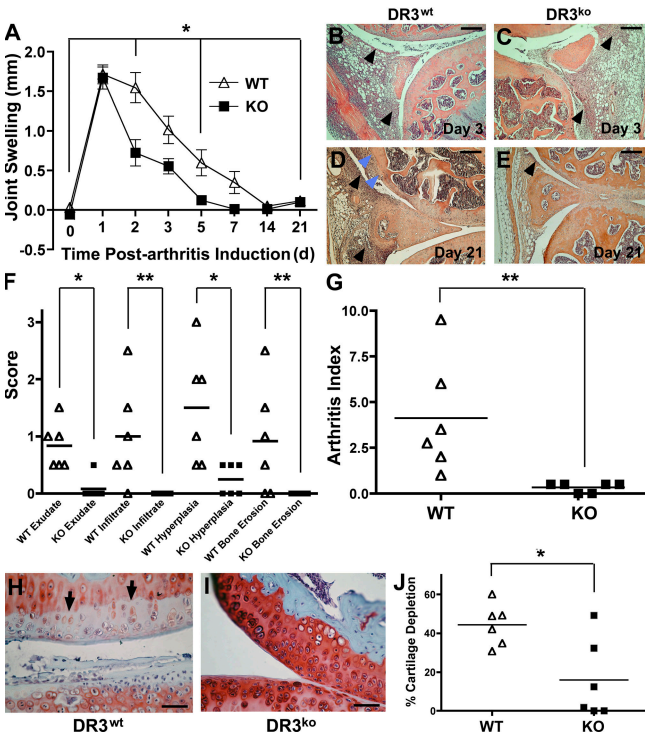

Figure 1. Protection against AIA in DR3^{ko} mice. (A) Joint swelling after intraarticular injection of mBSA. Data are mean ± SEM from $n = 6$ DR3^{wt} (△) or DR3^{ko} (■) mice. Two-way analysis of variance (ANOVA) shows significance at $P < 0.02$ (*). One representative experiment of three is shown. (B–E) Representative images from DR3^{wt} (B) and DR3^{ko} (C) mice, 3 d after arthritis induction, and DR3^{wt} (D) and DR3^{ko} (E) mice, 21 d after arthritis induction. Bars, 200 µm. Inflammatory tissue (black arrowheads) and erosions (blue arrowheads) are shown. (F) Breakdown of each component of the AI. *, $P < 0.05$; **, $P < 0.01$. (G) AI scores from DR3^{wt} and DR3^{ko} mice. **, $P < 0.01$. Lines mark means of graphed points. (H and I) Representative images of collagen around knee joints from DR3^{wt} (H) and DR3^{ko} (I) mice. Sections were stained with Safranin O/Fast Green to visualize collagen in red. Tidemark of cartilage depletion (arrows) is shown. Bars, 50 µm. (J) Estimated cartilage depletion from DR3^{wt} and DR3^{ko} mice. *, $P < 0.05$. Each point in the summary graphs represents a single 6 DR3^{wt} (△) or DR3^{ko} (■) animal.

quantities up to 100 ng. DR3^{het} mice were chosen as they showed intermediate AI scores compared with DR3^{wt} mice (Figs. 1 G and 2 A). Consequently, exacerbation or amelioration of disease after TL1A injection could be quantified, irrespective of the inherent variability in the model. Coadministration of TL1A resulted in significant dose-dependent exacerbation of disease in DR3^{het} mice (Fig. 2 A). This was strikingly illustrated by the effect on size of bone erosions and severity of bone destruction, which increased in a dose-dependent fashion after TL1A injection (Fig. 2, B and C). In contrast, TL1A had no significant effect on arthritis progression in DR3^{ko} mice over the concentration range studied (Fig. 2 D). Representative images of DR3^{ko} mice receiving 1 and 100 ng TL1A show the continued absence of bone erosions (Fig. 2, E and F). TL1A therefore exacerbates AIA and, in particular, adverse bone pathology in a DR3-dependent manner.

DR3 expression promotes osteoclastogenesis in AIA

Because DR3^{ko} mice were protected from the development of subchondral bone erosions in AIA, we elected to quantify the number of bone-resorbing osteoclasts within the joint at two distinct sites of epiphyseal bone. Osteoclasts are clearly visualized as large red multinucleated cells with tartrate-resistant acid phosphatase (TRAP). TRAP expression in DR3^{wt} and DR3^{ko} mice was comparable in the femoral head (Fig. 3, A–C) and growth plate (not depicted). However, in the periosteum at areas adjacent to pannus formation, where focal bone erosions could be visualized at high magnification, TRAP staining was significantly greater in DR3^{wt} mice than at equivalent areas in DR3^{ko} mice (Fig. 3, D–F). These data implicate a role for DR3 in generation of osteoclasts at sites of bone pathology but not in influencing osteoclastogenesis in areas away from the pannus.

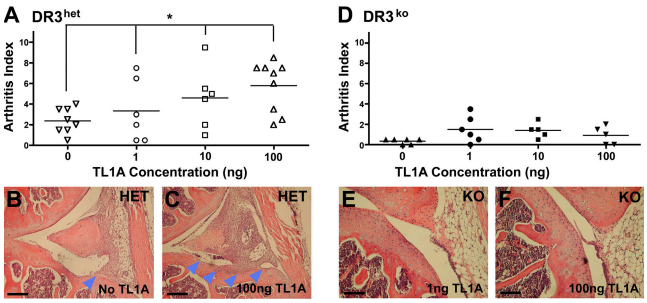

Figure 2. TL1A promotes adverse bone pathology of AIA in a DR3-dependent manner. (A) AI with increasing administration of TL1A in DR3^{het} mice. Horizontal lines mark means of graphed points. Open symbols represent DR3^{het} mice; filled symbols represent DR3^{ko} mice. (B and C) Representative images from DR3^{het} mice with no (B) or 100 ng (C) TL1A added. Bone erosions (arrowheads) are shown. (D) AI with increasing administration of TL1A to DR3^{ko} mice. (E and F) Representative images from DR3^{ko} mice with 1 (E) or 100 (F) ng TL1A added. Bars, 200 µm. One-way ANOVA showed significance of TL1A addition to DR3^{het} but not DR3^{ko} mice. *, $P < 0.05$. Each point in the summary graphs represents a single animal. One representative experiment of two is shown.

DR3^{ko} mice show normal myeloid infiltration within joints in AIA

Recruitment of mononuclear cells to the subintimal synovial lining layer and to periarticular adipose tissue adjacent to the meniscus is a process characteristic of the AIA model and RA patient joints. Indeed, the degree of macrophage (osteoclast precursor) infiltration within rheumatoid joint has been correlated with severity of structural damage in human disease. To assess whether reduction in osteoclast number was caused by impaired recruitment of these cells to the joint, we performed immunohistochemical analysis of F4/80 expression in sections from DR3^{ko} and DR3^{wt} mice on days 3 and 21 after arthritis induction. On day 3, some F4/80 expression was detected in the periarticular adipose tissue, which did not differ significantly between DR3^{wt} and DR3^{ko} mice (Fig. 3, G–I). By day 21, F4/80 staining was markedly increased with strong F4/80 expression visualized microscopically in both

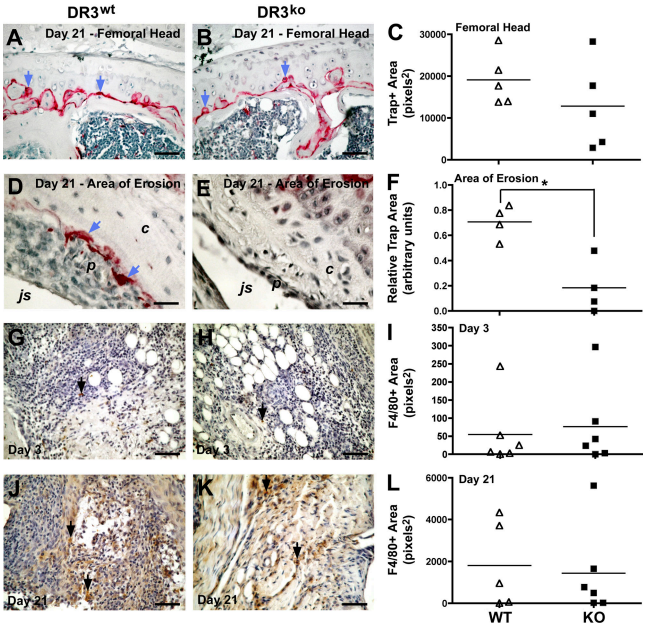

Figure 3. TRAP and F4/80 expression in joints of DR3^{wt} and DR3^{ko} mice. Sections were stained for TRAP or F4/80 as described in Materials and methods. Horizontal lines mark means of graphed points. (A and B) Representative images of TRAP staining at day 21 after arthritic induction from DR3^{wt} (A) and DR3^{ko} (B) mice. Red TRAP^{+} staining (arrows) is shown. (C) Summary of TRAP staining in femoral head at day 21. (D and E) Representative images of TRAP staining around areas of bone erosion at day 21 after arthritic induction from DR3^{wt} mice (D) and equivalent areas from DR3^{ko} mice (E). Red TRAP^{+} staining (arrows) is shown; *js*, joint space; *p*, pannus; *c*, cartilage. (F) DR3^{ko} mice show significantly reduced TRAP^{+} staining compared with DR3^{wt} mice. *, $P < 0.05$. (G and H) Representative images of F4/80 staining from DR3^{wt} (G) and DR3^{ko} (H) mice, 3 d after arthritis induction. (I) Summary of day-3 data. (J and K) Representative images of F4/80 staining from DR3^{wt} (J) and DR3^{ko} (K) mice, 21 d after induction of arthritis. F4/80-positive cells (arrows) are shown. (L) Summary of day-21 data. Each point in the summary graphs represents a single DR3^{wt} (△) or DR3^{ko} (■) animal. Bars, 50 µm. One representative experiment of two is shown.

DR3^{ko} and DR3^{wt} mice. Quantification of F4/80^{+} cells again revealed no significant difference in expression between DR3^{wt} and DR3^{ko} mice (Fig. 3, J–L). Overall, these data suggest that absence of DR3 does not impair recruitment of myeloid cells to the joint, nor does it affect overall numbers of basal mature osteoclasts in the femoral head. Neither hypothesis can explain the reduction in osteoclast numbers in areas of bone pathology in DR3^{ko} mice.

TL1A promotes osteoclastogenesis in vitro in a DR3-dependent fashion

We therefore tested the possibility that TL1A could directly promote differentiation of osteoclasts. To achieve this, we used an in vitro system of osteoclastogenesis from adherent BM-derived cells (BMC). BM macrophages (BMM) from DR3^{wt} mice were confirmed to express DR3 (Fig. 4 A). BMC from DR3^{wt} and DR3^{ko} mice did not differ in their ability to generate osteoclasts in the presence of soluble RANK-L and M-CSF as measured by the formation of multinucleated TRAP^{+} cells (Fig. 4 B). However, TL1A addition significantly enhanced development of osteoclasts from DR3^{wt} but not DR3^{ko} BMC (Fig. 4, B–D). TL1A in the absence of RANK-L and M-CSF could not generate osteoclasts (Fig. 4 E). The functional capacity of in vitro–generated osteoclasts to destroy bone was visualized by toluidine blue staining of pits in the ivory discs (Fig. 4 F). This data indicates that TL1A is not necessary for osteoclastogenesis per se, but promotes it in the presence of RANK-L and M-CSF and in a DR3-dependent fashion. In support of our murine data and highlighting the significance of these results for humans, TL1A significantly promoted osteoclastogenesis from monocytes derived from human peripheral blood (Fig. 4 G).

Anti-TL1A neutralizing antibody ameliorates AIA and CIA

To test the therapeutic potential of countering the DR3–TL1A pathway, we generated an antagonistic rat mAb to murine TL1A (Fig. 5, A and B) and applied it in AIA and the systemic model of disease. CIA is the industry standard for testing potential therapeutic agents against RA. A single treatment of anti-TL1A at the point of arthritic induction in AIA resulted in more rapid resolution of swelling that mirrored our observations in DR3^{ko} mice (Fig. 5 C). In CIA, clinical signs of arthritis became apparent in control mice on day 25 (Fig. 5 D). Disease activity was assessed by assigning scores to each paw according to degree of redness, swelling, and joint involvement. Paw scores in anti-TL1A–treated mice were consistently lower than in control IgG2a-treated mice, reaching significance on days 27 and 28 (Fig. 5 E). Disease activity in control IgG2a-treated mice was characterized by leukocyte infiltration of synovial tissues and variable degrees of bone erosion (Fig. 5 F). Specimens from anti-TL1A–treated mice demonstrated mild changes by comparison (Fig. 5 G). The AI in anti-TL1A–treated mice was significantly less than in IgG2a-treated controls (Fig. 5 H). These data are consistent with the protection against AIA observed in DR3^{ko} mice and suggest that countering the DR3–TL1A pathway may be therapeutic against RA in man.

The role of the DR3–TL1A axis in driving adverse bone pathology in inflammatory arthritis

Our findings show that DR3^{ko} mice are resistant to the adverse joint pathology that is typical in AIA and are consistent with an essential role for the DR3–TL1A pathway in development of inflammatory arthritis. DR3^{ko} mice elicited an initial inflammatory reaction in response to AIA induction, such that at day 3 after arthritis induction, there was no difference in histopathological scoring or level of inflammatory cell infiltrate between control and DR3^{ko} mice. Resolution of inflammation, however, occurred at a faster rate in DR3^{ko} mice, as indicated by reduction in joint swelling over the course of the study and reduction in all histopathological parameters measured at day 21 after arthritic induction. Of particular note was the absence of bone erosion and marked reduction in cell infiltrate in DR3^{ko} mice in later stages of disease. Comparable numbers of infiltrating F4/80^{+} macrophages were present in joints of DR3^{wt} and DR3^{ko} mice, despite the observed differences in joint pathology. Therefore, the mechanisms involved in initiating the inflammatory reaction and in recruitment of myeloid cells into the joint appear

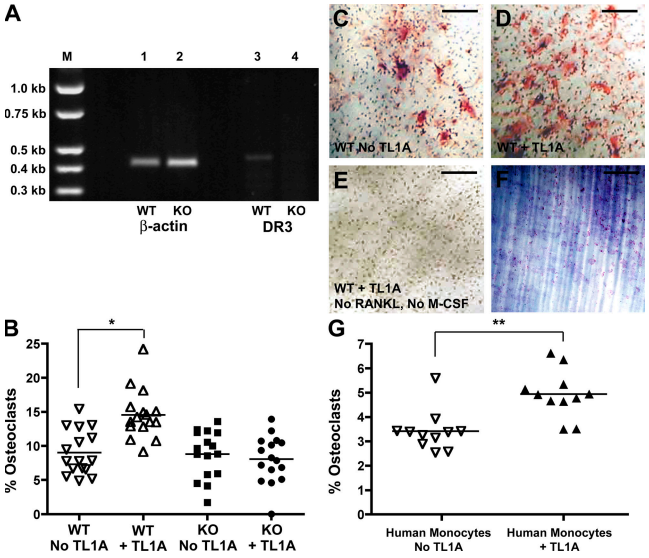

Figure 4. TL1A promotes DR3-dependent in vitro osteoclastogenesis. (A) RT-PCR of DR3 in BMM. In vitro osteoclastogenesis assays were performed as described in Materials and methods. Osteoclast numbers were estimated by counting multinucleated TRAP^{+} cells. (B) Effect of TL1A on proportion of osteoclasts generated in presence of RANKL and M-CSF. *, P = 0.0003. Each point represents a single ivory disc from experiments on DR3^{wt} (open symbols) or DR3^{ko} (filled symbols) mice. Four discs from four mice were counted for each treatment. Lines mark means of graphed points. One representative experiment of two is shown. (C–E) TRAP staining of BM cells from DR3^{wt} mice on discs with RANK-L + M-CSF and no TL1A (C) or 10 ng/ml TL1A (D) and TL1A (E), but no RANKL and M-CSF. Bars, 50 µm. (F) Toluidine blue staining of ivory discs showing pit-forming ability of osteoclasts generated in vitro. Bar, 150 µm. (G) Effect of TL1A on osteoclastogenesis from adherent human peripheral blood mononuclear cells and proportion of osteoclasts in cultures shown with (▽) or without (▲) exogenous TL1A added. **, P = 0.0013. One representative experiment of two is shown.

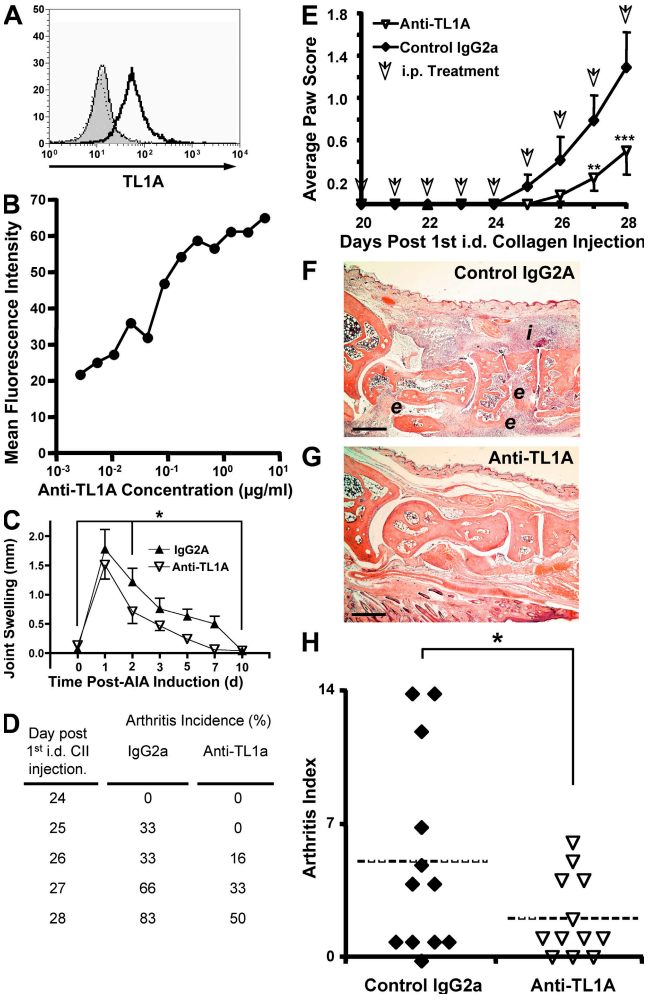

Figure 5. Early therapeutic intervention with anti-TL1A antibody arrests development of arthritis. (A) Binding of rat anti-TL1A mAb (TAN 2–2) to J558L cells transfected with plasmid encoding membrane-bound TL1A. Shaded histogram and dotted line represent binding of isotype control and TAN 2–2 to plasmid only transfected cells, respectively. Binding of isotype control and TAN 2–2 to TL1A-expressing cells is represented by a thin and thick line, respectively. (B) Titration of TAN 2–2 binding to J558L cells expressing membrane-bound TL1A. (C) Time course of swelling in AIA after anti-TL1A mAb treatment. Data are mean ± SEM from mice treated with control IgG2A (▲) or anti-TL1A (▽) mAb. One representative experiment of two is shown. *, $P < 0.02$ by two-way ANOVA. CIA was induced as described in Materials and methods. All data were derived from six mice for each treatment. (D) Arthritis incidence tabulated over 28-d time course. (E) Arthritis severity as a mean paw score from day 20 when dosing schedule for anti-TL1A and control IgG2a was started. Data are mean ± SEM. Timing of injections are shown (arrows). (F and G) Representative images of H&E-stained sections from control IgG2a (F) and anti-TL1A (G). *i*, intense synovial infiltration; *e*, aggressive bone erosion. Bars, 200 µm. (H) Analysis of AI of CIA in control IgG2a and anti-TL1A–treated mice. Dotted horizontal line depicts mean for each group. *, $P < 0.05$; **, $P = 0.01$; ***, $P = 0.006$.

intact in the absence of DR3. Because of this, we chose to investigate differentiation of osteoclasts, discovering that osteoclast differentiation in vitro and bone erosion in vivo was exacerbated by exogenous TL1A in control but not DR3^{ko} mice. These DR3-dependent effects confirm that TL1A is a specific functional ligand for DR3 and identifies the control of osteoclasts as a novel function for DR3. The potential of countering the DR3–TL1A pathway as a therapy was proven by amelioration of CIA and AIA using a neutralizing anti-TL1A mAb. Interestingly, anti-TL1A therapy was not totally protective. The possibility remains that there may be secondary ligands for DR3 and TL1A as implicated for TL1A by recent data in renal inflammation (22), but detailed studies have shown no other TNFSF/TNFRSF family members that bind murine DR3 or murine TL1A (18), whereas human TL1A binds Decoy Receptor 3 (11), a mouse homologue of which has not been found.

This is the first paper reporting that signaling through DR3 on myeloid cells promotes osteoclastogenesis, although it is clear from our data that it is not a prerequisite for, nor can it induce, this differentiation in the absence of RANK-L and M-CSF. In this respect, it mirrors functions that have been reported for TNFα (23). However, a function independent of TNFα is suggested by a recent paper showing that macrophages produce TL1A independent of TNF activity (20). TL1A expression, including release of active soluble forms of the protein, can be induced on human monocytes by FcγR stimulation through soluble (24) and insoluble immune complexes purified from RA synovial fluid (20). The majority of stromal macrophages in RA synovial tissue express TL1A, and in vitro stimulation of monocytes with PEG precipitates from RA samples results in production of nanogram quantities of soluble TL1A (20). This suggests very high levels in localized RA joint akin to the levels we used to exacerbate AIA (Fig. 2 A). The implication is that in inflammatory arthritis, myeloid cells may exhibit a positive feedback loop whereby TL1A is triggered through ICs and can drive differentiation of bone-destroying cells if the right cytokine milieu is provided. Intriguingly, TL1A also has varied effects on human osteoblast cell lines in vitro, inhibiting differentiation and promoting quiescence at low densities but inducing death at high densities (25). We therefore propose that the DR3–TL1A pathway may act as a switch that is capable of directly activating osteoclast but also inhibiting osteoblast differentiation and, in so doing, disregulate the homeostatic balance of degradation and formation in normal bone into the detrimental situation observed in destructive bone pathologies such as RA. Although our in vitro data supports this proposal, some caution is necessary in interpreting the contribution of direct TL1A-driven osteoclastogenesis to arthritic bone damage in vivo, as inflammation and bone erosion cannot be dissociated in AIA or CIA. The possibility remains that the resistance of DR3^{ko} mice to bone erosion is secondary to DR3–TL1A-dependent control of other parts of the inflammatory process.

In this respect, our data also show that cartilage depletion is significantly reduced in DR3^{ko} mice (Fig. 1). Cartilage depletion

is attributed to the effects of matrix metalloproteinases (MMPs), levels of which are raised in RA joint. In vitro experiments on human cell lines have shown that DR3 activation can induce the production of MMP-1, -9, and -13 in THP-1s (17). These MMPs have all been associated with RA joint pathology (26). In addition, it is also established that TL1A plays an important role in T cell function. TL1A has been shown to costimulate IL-2 responsiveness (11) and synergize with the TCR and IL-12/IL-18 pathways to induce IFNγ release (15, 27, 28). TL1A also amplifies cytokine release by NKT cells (14) and T cells (13) and regulates the development of proinflammatory Th17 cells (12, 16), which are reported to aid osteoclastogenesis in autoimmune arthritis (29). The action of TL1A on T cells may also be regulated by differential expression of splice variants of DR3 (27). The exact role of TL1A and DR3 on lymphocytes in inflammatory arthritis remains to be elucidated, but it is interesting to note that we find normal anti-mBSA Ab levels in serum, unchanged T cell proliferation to mBSA in draining lymph nodes of $DR3^{ko}$ mice after AIA induction, and normal in vitro generation of Th17 cells from $DR3^{ko}$ splenocytes (unpublished data).

In summary, we have induced inflammatory arthritis in $DR3^{ko}$ mice and found that they exhibit strong resistance to the adverse pathology observed in AIA. We show DR3-dependent TL1A-driven exacerbation of bone damage in vivo and promotion of osteoclastogenesis in vitro. We also show that anti-TL1A therapy ameliorates disease. Our data suggest that the DR3–TL1A pathway is an important component of inflammatory responses in joint disease and, as such, identifies a potential therapeutic target for treatment of diseases like RA but with potential impact in other diseases involving disrupted bone physiology.

MATERIALS AND METHODS

Animals. The DR3 mouse colony was founded from animals supplied by Cancer Research UK, London. All experiments were undertaken in male WT ($DR3^{wt}$), heterozygous ($DR3^{het}$), and KO ($DR3^{ko}$) mice, which have been described previously (10). DBA/1J mice were acquired from Harlan, UK. Animals were used at 6–8 wk of age. All procedures were approved by the Local Research Ethics Committee and performed in strict accordance with Home Office–approved licenses PPL 30/1999 and 30/2361.

Induction of murine AIA. AIA was induced as previously described (30). In brief, mice were s.c. immunized on two occasions, 1 wk apart, with 1 mg/ml mBSA with an equal volume of CFA. An additional i.p. injection of 100 μl of heat-inactivated *Bordetella pertussis* toxin was administered with the first immunization. AIA was induced in the hind right knee joint via an intraarticular injection of 10 mg/ml mBSA (6 μl), administered 21 d after the initial immunization. To assess the effect of TL1A or anti-TL1A administration, AIA was induced via mBSA injection in conjunction with 1, 10, or 100 ng of soluble TL1A (R&D Systems) or 100 ng of anti-TL1A mAb.

Generation of a rat anti–mouse TL1A monoclonal antibody. Rats were immunized with a soluble recombinant TL1A protein consisting of a human IgG1 Fc domain, with an additional hinge-like region at the C terminus, linked to the extracellular domain of mouse TL1A (T77-L252). The protein was produced in Chinese hamster ovary cells and was purified by immunoaffinity chromatography using an anti–human Fc mAb. Anti-TL1A mAb was generated by standard hybridoma technology and hybridoma supernatants were screened for binding to recombinant soluble and membrane-expressed TL1A. To generate cells expressing membrane-anchored TL1A, PCR fragments encoding the entire coding sequence of mouse TL1A were cloned into the mammalian expression vectors pEF1/V5-His A and pcDNA3.1 (Invitrogen), and plasmids were then transfected into J558L or 293T cells. Stable J558L cell lines expressing membrane-anchored TL1A were selected in Geneticin (400 μg/ml)-containing media. Splenic cDNA or IMAGE clone 30740802 was used as a template for PCR reactions to generate TL1A-encoding DNA fragments. Further selection of neutralizing anti-TL1A mAbs was based on the ability to block binding of soluble recombinant TL1A-Fc to anti-CD3/CD28–stimulated T cells.

Anti-TL1A therapy in CIA. CIA was induced as previously described (31). In brief, 2 mg/ml of chicken type II collagen (CII; Sigma-Aldrich) was emulsified with an equal volume of complete Freund's adjuvant and 100 μl of collagen/adjuvant mixture injected intradermally into several sites near the base of the tail of 7-wk-old male DBA/1J mice. A second identical booster was administered to each mouse 21 d after the first injection. The day of the first immunization was designated as day 0. Mice were randomly assigned to one of three treatment groups on day 20. Animals received nine daily 100-μl injections containing either 2.5 mg/kg of anti-TL1A or LEAF purified control rat IgG2a (Cambridge Biosciences) dissolved in sterile PBS or PBS alone administered by the i.p. route from day 20. Thereafter, arthritis incidence and severity was assessed daily until termination on day 28 when the disease severity limits were attained in IgG2a and PBS controls. The incidence of CIA was assessed as the percentage of mice developing arthritis among all mice. The severity of arthritis in each paw (paw score) was evaluated by using an established in-house scoring system: 0, normal; 1, mild but definite swelling in the ankle or wrist joint or redness and swelling limited to individual digits regardless of the number of digits affected; 2, moderate swelling of ankle or wrist; 3, severe redness and swelling of the ankle or wrist and proximal phalangeal joints; and 4, maximally inflamed limb with involvement of multiple joints, no ankylosis.

Assessment of arthritis. Joint swelling was assessed on days 1, 2, 3, 5, 7, 14, and 21 after arthritis induction by measuring the difference between hind right (AIA) and hind left (control) knee joint diameters using an analogue micrometer. Animals were killed on day 3 or 21 for assessment of inflammatory and pathological changes within the joint. Histological assessment was performed as previously described (30). All joints were fixed in neutral buffered formal saline and decalcified with 10% formic acid for 2 wk at 4°C before embedding in paraffin wax. Serial sections of 7-μm thickness were taken and stained routinely with H&E for analysis. Two blinded independent observers scored the sections for cellular infiltration (0–5), cellular exudate (0–3), synovial hyperplasia (0–3), and bone erosion (0–3), with 0 representing a normal joint. The sum of all parameters gave the AI. Sections were additionally stained with Safranin O and Fast Green to assess cartilage depletion.

RT-PCR. BMM were generated as previously described (32). RNA was extracted from BMM cultures using RNeasy (QIAGEN) after manufacturer's instructions, whereas cDNA was generated and RT-PCR performed according to standard Invitrogen protocols. PCR primers were as follows: β-actin, forward 5′-CGGCCAGGTCATCACTATTG-3′ and reverse 5′-CTCAGTAACCCGCCTAG-3′ giving a 410-bp product; and DR3, forward 5′-CTAAGGCTTGCACTGCTGTCT-3′ and reverse 5′-GAGCATCTCATACTGCTGGTC-3′ giving a 457-bp product. The PCR consisted of 33 cycles with a 59°C annealing temperature.

TRAP staining for osteoclasts. For TRAP staining, joints were decalcified in EDTA (7%), rehydrated, and incubated with TRAP staining solution containing 0.1 M acetate buffer, 0.5 M sodium tartrate, 10 mg/ml naphthol AS-MX phosphate, 100 μl Triton X-100, and 0.3 mg/ml Fast Red Violet LB salt for 3 h at 37°C. Sections were then counterstained with hematoxylin before mounting in DPX. Images were captured using a digital camera (N457; Olympus), and TRAP-positive cells were analyzed using Photoshop CS3. 5 (Adobe). Randomly chosen selected areas were used for analysis.

Immunohistochemistry for F4/80 expression. F4/80 expression was detected using an anti–rat HRP-DAB staining kit (R&D Systems) according to the manufacturer's instructions. In brief, sections were rehydrated and endogenous peroxidase activity was blocked. Antigen unmasking was achieved by incubating the sections in 0.1% prewarmed Trypsin/EDTA in PBS for 30 min at 37°C. After blocking steps, sections were incubated overnight with 4 μg/ml of rat anti-F4/80 antibody (Invitrogen) or isotype control diluted in PBS followed by secondary antibody as per the manufacturer's instructions. Positively labeled cells were visualized using a streptavidin-HRP conjugate and DAB chromogen. Sections were counterstained with hematoxylin, dehydrated, and mounted in DPX. Images were captured using a digital camera (N457), and F4/80 positive cells were analyzed using Photoshop. Randomly selected areas were used for analysis.

In vitro osteoclastogenesis assays. BMC were removed from femurs of $DR3^{wt}$ and $DR3^{ko}$ mice by centrifugation after removal of the proximal end. BMC were resuspended in α-MEM supplemented with 10% FCS, 2 mM L-glutamine, and antibiotics (MEM-10) and 5×10^5 cells added to ivory discs. After 2 h at 37°C, nonadherent cells were removed by transfer of ivory discs to new wells with fresh media supplemented with 50 ng/ml RANKL and 25 ng/ml M-CSF with or without 10 ng/ml TL1A. All media were replenished after 3 d. TRAP staining was performed according to the manufacturer's instructions (Sigma-Aldrich) after 7 d. Six fields of view on each disc were counted for TRAP-positive multinucleated cells. For human osteoclastogenesis assays, peripheral blood mononuclear cells were used as a source for adherent cells and cultures were maintained for 21 d before TRAP staining.

Statistical analysis. Readouts could not be assumed to be normally distributed as they were histological scores or percentages. Therefore, nonparametric Mann-Whitney *U* tests were used for statistical analysis. One-way unpaired and two-way ANOVAs were used when testing the influence of third parameters such as time or dose. Analyses were performed on GraphPad Prizm v4. P-values of ≤0.05 were considered significant and values of ≤0.01 were considered highly significant.

This work was funded by the Medical Research Council, through a Medical Research Council Career Establishment Grant awarded to E.C.Y. Wang (G0300180), a Medical Research Council Collaboration Grant (G0500617), the Wellcome Trust and two PhD studentships, one part-funded by the I3-Interdisciplinary Research Group, Cardiff University.

The authors have no conflicting financial interests.

Submitted: 6 November 2007
Accepted: 2 September 2008

REFERENCES

1. Feldmann, M., F.M. Brennan, and R.N. Maini. 1996. Rheumatoid arthritis. *Cell*. 85:307–310.
2. Williams, R.O., M. Feldmann, and R.N. Maini. 1992. Anti-tumor necrosis factor ameliorates joint disease in murine collagen-induced arthritis. *Proc. Natl. Acad. Sci. USA*. 89:9784–9788.
3. Abramson, S.B., and A. Amin. 2002. Blocking the effects of IL-1 in rheumatoid arthritis protects bone and cartilage. *Rheumatology (Oxford)*. 41:972–980.
4. Boe, A., M. Baiocchi, M. Carbonatto, R. Papoian, and O. Serlupi-Crescenzi. 1999. Interleukin 6 knock-out mice are resistant to antigen-induced experimental arthritis. *Cytokine*. 11:1057–1064.
5. Asagiri, M., and H. Takayanagi. 2007. The molecular understanding of osteoclast differentiation. *Bone*. 40:251–264.
6. Kitson, J., T. Raven, Y.P. Jiang, D.V. Goeddel, K.M. Giles, K.T. Pun, C.J. Grinham, R. Brown, and S.N. Farrow. 1996. A death-domain-containing receptor that mediates apoptosis. *Nature*. 384:372–375.
7. Bodmer, J.L., K. Burns, P. Schneider, K. Hofmann, V. Steiner, M. Thome, T. Bornand, M. Hahne, M. Schroter, K. Becker, et al. 1997. TRAMP, a novel apoptosis-mediating receptor with sequence homology to tumor necrosis factor receptor 1 and Fas(Apo-1/CD95). *Immunity*. 6:79–88.
8. Screaton, G.R., X.N. Xu, A.L. Olsen, A.E. Cowper, R. Tan, A.J. McMichael, and J.I. Bell. 1997. LARD: a new lymphoid-specific death domain containing receptor regulated by alternative pre-mRNA splicing. *Proc. Natl. Acad. Sci. USA*. 94:4615–4619.
9. Marsters, S.A., J.P. Sheridan, C.J. Donahue, R.M. Pitti, C.L. Gray, A.D. Goddard, K.D. Bauer, and A. Ashkenazi. 1996. Apo-3, a new member of the tumor necrosis factor receptor family, contains a death domain and activates apoptosis and NF-kappa B. *Curr. Biol*. 6:1669–1676.
10. Wang, E.C., A. Thern, A. Denzel, J. Kitson, S.N. Farrow, and M.J. Owen. 2001. DR3 regulates negative selection during thymocyte development. *Mol. Cell. Biol*. 21:3451–3461.
11. Migone, T.S., J. Zhang, X. Luo, L. Zhuang, C. Chen, B. Hu, J.S. Hong, J.W. Perry, S.F. Chen, J.X. Zhou, et al. 2002. TL1A is a TNF-like ligand for DR3 and TR6/DcR3 and functions as a T cell costimulator. *Immunity*. 16:479–492.
12. Pappu, B.P., A. Borodovsky, T.S. Zheng, X. Yang, P. Wu, X. Dong, S. Weng, B. Browning, M.L. Scott, L. Ma, et al. 2008. TL1A-DR3 interaction regulates Th17 cell function and Th17–mediated autoimmune disease. *J. Exp. Med*. 205:1049–1062.
13. Meylan, F., T.S. Davidson, E. Kahle, M. Kinder, K. Acharya, D. Jankovic, V. Bundoc, M. Hodges, E.M. Shevach, A. Keane-Myers, et al. 2008. The TNF-family receptor DR3 is essential for diverse T cell-mediated inflammatory diseases. *Immunity*. 29:79–89.
14. Fang, L., B. Adkins, V. Deyev, and E.R. Podack. 2008. Essential role of TNF receptor superfamily 25 (TNFRSF25) in the development of allergic lung inflammation. *J. Exp. Med*. 205:1037–1048.
15. Bamias, G., C. Martin III, M. Marini, S. Hoang, M. Mishina, W.G. Ross, M.A. Sachedina, C.M. Friel, J. Mize, S.J. Bickston, et al. 2003. Expression, localization, and functional activity of TL1A, a novel Th1-polarizing cytokine in inflammatory bowel disease. *J. Immunol*. 171:4868–4874.
16. Takedatsu, H., K.S. Michelsen, B. Wei, C.J. Landers, L.S. Thomas, D. Dhall, J. Braun, and S.R. Targan. 2008. TL1A (TNFSF15) regulates the development of chronic colitis by modulating both T-Helper 1 and T-Helper 17 activation. *Gastroenterology*. 135:552–567.
17. Kang, Y.J., W.J. Kim, H.U. Bae, D.I. Kim, Y.B. Park, J.E. Park, B.S. Kwon, and W.H. Lee. 2005. Involvement of TL1A and DR3 in induction of pro-inflammatory cytokines and matrix metalloproteinase-9 in atherogenesis. *Cytokine*. 29:229–235.
18. Bossen, C., K. Ingold, A. Tardivel, J.L. Bodmer, O. Gaide, S. Hertig, C. Ambrose, J. Tschopp, and P. Schneider. 2006. Interactions of tumor necrosis factor (TNF) and TNF receptor family members in the mouse and human. *J. Biol. Chem*. 281:13964–13971.
19. Osawa, K., N. Takami, K. Shiozawa, A. Hashiramoto, and S. Shiozawa. 2004. Death receptor 3 (DR3) gene duplication in a chromosome region 1p36.3: gene duplication is more prevalent in rheumatoid arthritis. *Genes Immun*. 5:439–443.
20. Cassatella, M.A., G.P. da Silva, I. Tinazzi, F. Facchetti, P. Scapini, F. Calzetti, N. Tamassia, P. Wei, B. Nardelli, V. Roschke, et al. 2007. Soluble TNF-like cytokine (TL1A) production by immune complexes stimulated monocytes in rheumatoid arthritis. *J. Immunol*. 178:7325–7333.
21. Simon, J., R. Surber, G. Kleinstauber, P.K. Petrow, S. Henzgen, R.W. Kinne, and R. Brauer. 2001. Systemic macrophage activation in locally-induced experimental arthritis. *J. Autoimmun*. 17:127–136.
22. Al-Lamki, R.S., J. Wang, A.M. Tolkovsky, J.A. Bradley, J.L. Griffin, S. Thiru, E.C. Wang, E. Bolton, W. Min, P. Moore, et al. 2008. TL1A both promotes and protects from renal inflammation and injury. *J. Am. Soc. Nephrol*. 19:953–960.
23. Lam, J., S. Takeshita, J.E. Barker, O. Kanagawa, F.P. Ross, and S.L. Teitelbaum. 2000. TNF-alpha induces osteoclastogenesis by direct stimulation of macrophages exposed to permissive levels of RANK ligand. *J. Clin. Invest*. 106:1481–1488.
24. Prehn, J.L., L.S. Thomas, C.J. Landers, Q.T. Yu, K.S. Michelsen, and S.R. Targan. 2007. The T cell costimulator TL1A is induced by FcgammaR signaling in human monocytes and dendritic cells. *J. Immunol*. 178:4033–4038.
25. Borysenko, C.W., V. Garcia-Palacios, R.D. Griswold, Y. Li, A.K. Iyer, B.B. Yaroslavskiy, A.C. Sharrow, and H.C. Blair. 2006. Death receptor-3 mediates apoptosis in human osteoblasts under narrowly regulated conditions. *J. Cell. Physiol*. 209:1021–1028.

26. Burrage, P.S., K.S. Mix, and C.E. Brinckerhoff. 2006. Matrix metalloproteinases: role in arthritis. *Front. Biosci.* 11:529–543.
27. Bamias, G., M. Mishina, M. Nyce, W.G. Ross, G. Kollias, J. Rivera-Nieves, T.T. Pizarro, and F. Cominelli. 2006. Role of TL1A and its receptor DR3 in two models of chronic murine ileitis. *Proc. Natl. Acad. Sci. USA.* 103:8441–8446.
28. Papadakis, K.A., D. Zhu, J.L. Prehn, C. Landers, A. Avanesyan, G. Lafkas, and S.R. Targan. 2005. Dominant role for TL1A/DR3 pathway in IL-12 plus IL-18-induced IFN-gamma production by peripheral blood and mucosal CCR9+ T lymphocytes. *J. Immunol.* 174:4985–4990.
29. Sato, K., A. Suematsu, K. Okamoto, A. Yamaguchi, Y. Morishita, Y. Kadono, S. Tanaka, T. Kodama, S. Akira, Y. Iwakura, et al. 2006. Th17 functions as an osteoclastogenic helper T cell subset that links T cell activation and bone destruction. *J. Exp. Med.* 203:2673–2682.
30. Williams, A.S., M. Mizuno, P.J. Richards, D.S. Holt, and B.P. Morgan. 2004. Deletion of the gene encoding CD59a in mice increases disease severity in a murine model of rheumatoid arthritis. *Arthritis Rheum.* 50: 3035–3044.
31. Campbell, I.K., J.A. Hamilton, and I.P. Wicks. 2000. Collagen-induced arthritis in C57BL/6 (H-2b) mice: new insights into an important disease model of rheumatoid arthritis. *Eur. J. Immunol.* 30:1568–1575.
32. Calder, C.J., L.B. Nicholson, and A.D. Dick. 2005. A selective role for the TNF p55 receptor in autocrine signaling following IFN-gamma stimulation in experimental autoimmune uveoretinitis. *J. Immunol.* 175:6286–6293.